**Earth System Dynamics**
Discussions

Open Access

# Inter-annual and seasonal trends of vegetation condition in the Upper Blue Nile (Abbay) basin: dual scale time series analysis

E. Teferi[1,2,3], S. Uhlenbrook[1,2], and W. Bewket[4]

[1]UNESCO-IHE Institute for Water Education, P.O. Box 3015, 2601 DA Delft, the Netherlands
[2]Delft University of Technology, Water Resources Section, P.O. Box 5048, GA Delft, the Netherlands
[3]College of Development Studies, Addis Ababa University, P.O. Box 2176, Addis Ababa, Ethiopia
[4]Department of Geography and Environmental Studies, Addis Ababa University, P.O. Box 2176, Addis Ababa, Ethiopia

Correspondence to: E. Teferi (ermias52003@yahoo.com)

---

Discussion Paper | Discussion Paper | Discussion Paper | Discussion Paper

ESDD
6, 169–216, 2015

Inter-annual and seasonal trends of vegetation

E. Teferi et al.

Title Page

Abstract | Introduction
Conclusions | References
Tables | Figures

|◄ | ►|
◄ | ►
Back | Close

Full Screen / Esc

Printer-friendly Version

Interactive Discussion

Title Page

Abstract    Introduction

Conclusions    References

Tables    Figures

|◄    ►|

◄    ►

Back    Close

Full Screen / Esc

Printer-friendly Version

Interactive Discussion

# Abstract

A long-term decline in ecosystem functioning and productivity, often called land degradation, is a serious environmental and development challenge to Ethiopia that needs to be understood so as to develop sustainable land use strategies. This study examines inter-annual and seasonal trends of vegetation cover in the Upper Blue Nile (UBN) or Abbay basin. Advanced Very High Resolution Radiometer (AVHRR) based Global Inventory, Monitoring, and Modelling Studies (GIMMS) Normalized Difference Vegetation Index (NDVI) was used for course scale long-term vegetation trend analysis. Moderate-resolution Imaging Spectroradiometer (MODIS) NDVI data (MOD13Q1) was used for finer scale vegetation trend analysis. Harmonic analyses and non-parametric trend tests were applied to both GIMMS NDVI (1981–2006) and MODIS NDVI (2001–2011) data sets. Based on a robust trend estimator (Theil–Sen slope) most part of the UBN ($\sim 77\%$) showed a positive trend in monthly GIMMS NDVI with a mean rate of 0.0015 NDVI units ($3.77\% \, \text{yr}^{-1}$), out of which 41.15 % of the basin depicted significant increases ($P < 0.05$) with a mean rate of 0.0023 NDVI units ($5.59\% \, \text{yr}^{-1}$) during the period. However, the finer scale (250 m) MODIS-based vegetation trend analysis revealed that about 36 % of the UBN shows a significantly decreasing trend ($P < 0.05$) over the period 2001–2011 at an average rate of 0.0768 NDVI $\text{yr}^{-1}$. This indicates that the greening trend of vegetation condition was followed by browning trend since the mid-2000s in the basin, which requires the attention of land users and decision makers. Seasonal trend analysis was found to be very useful in identifying changes in vegetation condition that could be masked if only inter-annual vegetation trend analysis was performed. The finer scale intra-annual trend analysis revealed trends that were more linked to human activities. This study concludes that integrated analysis of course and fine scale, inter-annual and intra-annual trends enables a more robust identification of changes in vegetation condition.

# 1 Introduction

Land degradation is a widespread environmental and development challenge (e.g. Dregne et al., 1991; UNEP, 2007). It is central to many international conventions and protocols related to environmental protection. Increasing demands for food, water and energy resulting from the growth in population and *per capita* consumption are driving unprecedented land use change (Godfray et al., 2010; Kearney, 2010). In turn, unsustainable land use is causing degradation of land resources. Thus, up-to-date quantitative information about land degradation is crucial to develop sustainable land use strategies and to support policy development for food and water security and environmental integrity. Status and trend of vegetation condition generally serve as a proxy for land degradation (Metternicht et al., 2010; Wessels et al., 2004, 2007).

Detecting and characterizing trends in vegetation condition over time using remotely sensed data has received considerable attention in recent years (Bai et al., 2008; de Jong et al., 2011; Eastman et al., 2013; Verbesselt et al., 2010a). Recent interest in vegetation trend analysis arises for three reasons. First, there is considerable interest in monitoring and assessing the state and trend of land degradation as well as for monitoring the performance of management programs (Buenemann et al., 2011; Vogt et al., 2011). Second, it is only recently that substantial amounts of remotely sensed data and robust geospatial approaches suitable to such analysis are becoming available (Bai et al., 2008; Buenemann et al., 2011; Tucker et al., 2005). Third, it is a natural first step toward identifying drivers of changes in terrestrial ecosystems as vegetation variability and trends affect the exchange of water, energy, nutrients and carbon between the biosphere, the geosphere and the atmosphere (Baldocchi et al., 2001).

Long-term, remotely sensed normalized difference vegetation index (NDVI) data are suitable to detect and characterize trends in vegetation condition over time (de Jong et al., 2011; Eastman et al., 2013; Tucker et al., 2001; Verbesselt et al., 2010a). Although NDVI can be computed from different multispectral satellite data, NDVI from Advanced Very High Resolution Radiometer (AVHRR) is the only global vegetation dataset which

spans a time period of three decades. Hence, it allows quantification of ecosystem changes as a result of ecosystem dynamics and varying climate conditions. In this study, AVHRR based Global Inventory, Monitoring, and Modelling Studies (GIMMS) NDVI data sets (1981–2006) were used for the purpose of long-term trend analysis (Tucker et al., 2005). Besides, NDVI time series (2001–2011) from the Moderate resolution Imaging Spectroradiometer (MODIS) 250 m (MOD13Q1) on board the Earth Observing System Terra platform were used for fine scale vegetation trend analysis.

In general, trends in vegetation occur in two ways: first, a gradual change over time that is consistent in direction (monotonic) such as change in land management or land degradation or, second, an abrupt shift at a specific point in time (step trend) that may be caused by disturbances such as a sudden change in land use policies, deforestation, floods, droughts, and fires (e.g. de Jong et al., 2013; Verbesselt et al., 2010b). Detecting a significantly increasing or decreasing pixel is not enough to assess the environmental impact or to be able to attribute the change to drivers behind. Abrupt changes or interruptions of trends may occur within the long-term vegetation time series (Angert et al., 2005; Slayback et al., 2003; Tucker et al., 2001).

Several vegetation trend studies from analysis of satellite observations have reported increasing trend of greenness in the Northern Hemisphere, including the Sahel (Fensholt et al., 2009; Karlsen et al., 2007; Slayback et al., 2003; Tucker et al., 2001). Other studies based on phenology and temperature observations from stations also confirmed greenness trends (Menzel et al., 2006; Sparks et al., 2009). However, Zhao and Running (2010) reported a decreasing trend in greenness globally during the period 2000–2009 using Moderate-resolution Imaging Spectroradiometer (MODIS) NDVI data. Similarly, de Jong et al. (2011) found that many forested biomes experienced a decline in vegetation greenness. There is still no consistent result on trends of global vegetation activity (Bala et al., 2013).

The inconsistent results from various studies potentially emanated from differences in location of study areas (variations in altitude and latitude), trend detection techniques (ordinary least square versus median trend), the length of the data series and NDVI

**Inter-annual and seasonal trends of vegetation**

E. Teferi et al.

Title Page

Abstract | Introduction

Conclusions | References

Tables | Figures

◄ | ►

◄ | ►

Back | Close

Full Screen / Esc

Printer-friendly Version

Interactive Discussion

data sources used (e.g. GIMMS, MODIS). Therefore, it is very important to characterize and understand inter-annual and intra-annual variability of vegetation activity using long-term data sets in study areas such as Abbay basin (1982–2006) where climate variability is high and topography is diverse.

5    It is essential to characterize and understand inter-annual and intra-annual variability of vegetation activity using long-term data sets such as GIMMS NDVI, especially, if the increase or decrease of vegetation growth in Abbay basin is mainly driven by climatic factors (De Beurs et al., 2009). However, if vegetation growth is mainly caused by human activities such as sustainable land management (SLM) programs that in-
10  volve localized implementation of best management practices (BMPs), then it is useful to use MODIS NDVI data as it provides frequent information at the spatial scale at which most human-driven land cover changes occur (De Beurs et al., 2009; Gallo et al., 2005; Townshend and Justice, 1988). Such analysis reveals areas of change that merit closer attention since it depicts significant shifts in local water, carbon and energy
15  fluxes (Henebry, 2009; Vuichard et al., 2008).

The general objective of this study was to characterize the degree of improvement or degradation of vegetation condition in the Abay basin using both coarse and fine scale analysis. The specific objectives were: (1) to identify inter-annual and seasonal trends in vegetation conditions at both coarse and fine scales using robust trend estimators;
20  and (2) to detect trend breaks.

## 2   Materials and methods

### 2.1   Study area

The Upper Blue Nile/Abbay basin covers a total area of 199 812 km$^2$ and is located in the center and west of Ethiopia. It lies approximately between $7°45'$ and
25  $12°46'$ N, and $34°06'$ and $40°00'$ E. Altitude of the Upper Blue Nile basin ranges from 475 m asl at the Sudanese border to 4257 m a.s.l. at the summit of Mt. Guna.

More than 83 % of the basin is located at an elevation above 1000 m a.s.l. Cropland is the major land use and land cover type, occupying more than 44 % of the total area of the basin (TECSULT, 2004). The multi-year (1983–2006) mean annual rainfall varies between about 894 to 1909 mm a$^{-1}$, with a spatial mean of about 1396 mm a$^{-1}$ based on gridded station-based rainfall data. The multi-year (1982–2006) mean annual areal potential evaporation ranges from 1065 to 1756 mm a$^{-1}$, with a spatial mean of about 1396 mm a$^{-1}$ based on the Penman–Monteith method from Climate Research Unit (CRU) 3.10 data set (Harris et al., 2014). The multi-year (1982–2006) annual average temperature varies across space from 14 to 29 °C based on CRU 3.10 data set.

## 2.2   Data sets

### 2.2.1   GIMMS 15-day composite NDVI product

The Global Inventory, Monitoring, and Modelling Studies (GIMMS) NDVI data product (Tucker et al., 2005), was used to analyze the long-term (1982–2006) vegetation variability and trends in UBN basin. A release of the global coverage GIMMS data (GIMMSg) at 8 km resolution, covering from July 1981 through December 2006, was made freely available from the Global Land Cover Facility of the University of Maryland (www.landcover.org). Recently an updated GIMMS NDVI dataset (GIMMS3g) covering from 1981 to 2010 has been processed by the GIMMS research group. In this study, due to the ease of accessibility of the data set, the GIMMSg NDVI data set was used. The GIMMSg data set is composited at a 15-day time step by applying maximum value compositing (MVC) technique (Holben, 1986) in order to reduce cloud cover and water vapor effects. The GIMMSg NDVI data set was cut to the extent of Abay basin and the bimonthly data were aggregated to monthly composites by applying the arithmetic mean of each month.

### 2.2.2 MODIS NDVI 16-Day L3 Global 250 m (MOD13Q1)

The MODIS 16-day composite NDVI data sets with 250 m spatial resolution (MOD13Q1) tiles of h21v07 and h21v08 for the period 2001–2011 obtained from the NASA Earth Observing System (EOS) data gateway were used in this study (Huete et al., 2002). The MODIS NDVI complements NOAA's AVHRR derived NDVI products and provides continuity for time series historical applications. The MODIS NDVI products are computed from atmospherically corrected bi-directional surface reflectances that have been masked for water, clouds, heavy aerosols and cloud shadows.

### 2.2.3 Land use and land cover *(LULC)* data

The third data set used in the analysis was *LULC* data produced by Woody Biomass Inventory and Strategic Planning Project (WBISPP) at a scale of 1 : 250 000 (TEC-SULT, 2004). The intention was to provide a basis for understanding the spatial distribution of seasonal trends.

### 2.3 Harmonic analysis of NDVI time-series

Both AVHRR and MODIS NDVIs are composite products. Since Maximum Value Composite (MVC) is not an atmospheric-correction method, some artefacts related to residual cloud cover and atmospheric haze remain in the MVC processed NDVI series (Nagol et al., 2009). Therefore, it was essential to perform harmonic analysis of both GIMMSg and MDOIS NDVI data sets using HANTS (Harmonic Analysis of Time Series) algorithm (Roerink et al., 2000; Verhoef et al., 1996) for the purpose of: (i) screening and removal of cloud contaminated observations; and (ii) temporal interpolation of the remaining observations to reconstruct gapless images at a prescribed time. Harmonic (Fourier) analysis has been successfully applied to describing precipitation patterns (e.g.Landin and Bosart, 1989), meteorology (e.g. Legates and Willmott, 1990) and seasonal and interannual variations in land surface condition (Jakubauskas et

al., 2001). The HANTS algorithm was developed based on the concept of Discrete Fourier Transform. HANTS considers only the most significant frequencies expected to be present in the time profiles, and applies a least squares curve fitting procedure based on harmonic components (sine and cosine). Thus, harmonic (Fourier) analysis decomposes a time-dependent periodic phenomenon (e.g. vegetation development) into a series of sinusoidal functions, each defined by unique amplitude (strength) and phase (orientation with respect to time) (Roerink et al., 2000; Verhoef et al., 1996) and can be described as the sum of sine and cosine components as follows (Harris and Stöcker, 1998; Wilks, 2011):

$$f(t) = \alpha_0 + \sum_{n=1}^{n=2} C_n \cos(\omega_n t - \varphi_n) \tag{1a}$$

$$= \alpha_0 + \sum_{n=1}^{n=2} \left\{ a_n \sin\left(\frac{2\pi n t}{T}\right) + b_n \cos\left(\frac{2\pi n t}{T}\right) \right\} + e \tag{1b}$$

where $f(t)$ is the series value at time $t$, $T$ is the length of the series (e.g. $T = 12$ observations for a monthly time series), $n$ is the number of harmonics to be used in the regression (in this study 2 harmonics were used), $\alpha_0$ is the mean of the series, $C_n$ is the amplitude of harmonics given by $C_n = \sqrt{a_n^2 + b_n^2}$, $\omega_n$ is the frequency ($2\pi n/T$), $\varphi_n$ is the phase angle given by $\varphi_n = \tan^{-1}(b_n/a_n)$ and $e$ is the error term. Equation (1a) emphasizes the harmonic interpretation, while Eq. (1b) is a convenient transformation to a multiple linear harmonic regression model with coefficients $a_n = C_n \cos(\varphi_n)$ and $b_n = C_n \sin(\varphi_n)$ that can be easily estimated.

In this study the IDL implementation of the HANTS algorithm (De Wit and Su, 2005) was used. Essential HANTS parameters were set as in Table 1 in order to obtain a reliable fitting curve. Detail explanation about the parameters can be found in Roerink et al. (2000). The zero frequency (mean annual NDVI) and the frequencies with time

periods of 1 year (annual) and 6 months (semi-annual) were selected for the analysis. So the output comprises five Fourier components (i.e. 3 amplitudes and 2 phases).

## 2.4 Long-term trend analysis

Before the time series analysis the biweekly HANTS filtered GIMMS and MODIS data were aggregated to monthly composites by applying the arithmetic mean of each month. Seasonal variation must be removed in order to better discern the long-term trend in NDVI over time. Thus, a seasonally adjusted series is needed in order to better discern any trend that might otherwise be masked by seasonal variation. Standardized anomalies ($Z$ score) of the monthly HANTS filtered NDVI data were calculated to remove the seasonality from the original time series (i.e. *de-seasoning*) using the following equation:

$$Z = (x - \mu)/\sigma \tag{2}$$

where $x$ is the data value of the respective month, $\mu$ is the monthly long term average value (i.e., the long term average of all Januaries, Februaries, . . . ) and $\sigma$ is the monthly standard deviation. A $Z$ score value of 0 would mean that it has a value equal to the long-term mean; a value of +1 would mean that it is 1 standard deviation of the long term mean, and so on.

The de-seasoned monthly NDVI time-series was corrected for serial correlation (autocorrelation) using a Trend Preserving Prewhitening (TPP) approach (Wang and Swail, 2001). The prewhitened series has the same trend as the original series, but with no serial correlation. Three types of inter-annual trend analysis and one trend significance test were applied to pre-whitened data on a pixel basis: linear trend (ordinary least squares regression (OLS)), median trend (Theil–Sen), monotonic trend (Mann–Kendall) and Mann–Kendall significance. The presence of a linear trend was tested by both linear trend (OLS) and median trend (Theil–Sen) operators. The linear trend (OLS) trend operator computes the slope coefficient of an ordinary least squares regression between the values of each pixel over time and a perfectly linear series. If a plot of

NDVI data ($Y$) versus time ($t$) suggests a simple linear increase or decrease over time, a simple linear regression of $Y$ on time $t$ is a test for linear trend: $Y = \beta_0 + \beta_1 t + e$ where $\beta_0$ is the intercept, $\beta_1$ is the slope coefficient, and $e$ is the error term. The $t$-statistic may be used to determine if the slope coefficient $\beta_1$ is significantly different from zero. However, the slope computed in this way is sensitive to outliers in the data and the data need to be normally distributed. Therefore, a robust non-parametric operator, the median trend (Theil–Sen (TS)) was computed for assessing the linear trend and rate of change per unit time (Hoaglin et al., 1983). Theil–Sen (TS) slope estimator was proposed by Thiel (1950) and modified by Sen (1968) and computes the median of the slopes between observation values at all pair-wise time steps given by the following equation:

$$\beta_1 = \text{median} \left( \frac{y_j - y_i}{x_j - x_i} \right) \tag{3}$$

for all $i < j$ and $i = 1, 2, \ldots, n - 1$ and $j = 2, 3, \ldots, n$.

The major advantage of TS slope estimator is because of its breakdown bound. The breakdown bound for a robust statistic is the number of wild values that can occur within a series before it will be affected. For the median trend, the breakdown bound is approximately 29 %, meaning that the trends expressed in the image must have persisted for more than 29 % of the length of the series (in time steps). For example, in this study the time series data contains 300 monthly images so it is completely unaffected by wild and noisy values unless they persist for more than 87 months (i.e. $0.29 \times 300 = 7.25$ years). The implication of this is that it also ignores the effects of short-term inter-annual climate teleconnections such as El Niño (typically a 12 months effect) and La Niña (typically a 12–24 months effect).

The non-linear trend was tested by mapping the degree of trend monotonicity (using the Mann–Kendall statistic) – the degree to which the trend is consistently increasing or decreasing. The significance of the trend was assessed using the non-parametric Mann–Kendall test.

**Inter-annual and seasonal trends of vegetation**

E. Teferi et al.

Title Page

Abstract | Introduction

Conclusions | References

Tables | Figures

|◀ | ▶|

◀ | ▶

Back | Close

Full Screen / Esc

Printer-friendly Version

Interactive Discussion

## 2.5 Seasonal trend analysis

Seasonal trend analysis was performed in order to identify trends in the essential character of the seasonal cycle while rejecting noise and short-term variability seasonal cycle (Eastman et al., 2013). This was performed based on a two-stage time series

5 analysis. First, harmonic regression is applied to each year of images in the time series to extract images of harmonic series shape parameters. Apart from the zero frequency, the number of frequency used in this study was two. Therefore, five time series images for each year in the series were produced, namely, the mean annual (Amplitude 0), the annual cycle (Amplitude 1 and Phase 1) and the semi-annual cycle images (Ampli-

10 tude 2 and Phase 2). In doing so, the high frequency variation such as that introduced by noise and short-term climate variability such as the Madden–Julian Oscillation are removed (Madden and Julian, 1971). Second, trends over years in these five harmonic series shape parameters were analyzed using a Theil–Sen median slope operator. This procedure is robust to short-term interannual variability up to a period of 29 % of the

15 length of the series (Eastman et al., 2013; Gilbert, 1987; Hoaglin et al., 1983). Furthermore, the samples are annual measures of shape parameters. Thus, short inter-annual disturbances (i.e. those 8 years or less in this case) such as individual El Niño/Southern Oscillation (ENSO) events, have little effect on the long-term trends represented by the median trends. The significance of the trends in the five shape parameters was

20 tested using the Contextual Mann Kendall statistics (CMK) (Neeti and Eastman, 2011) which is a modified form of the Mann–Kendall test of trend significance (Kendall, 1948; Mann, 1945).

Amplitude trend image was created by color compositing trends in Amplitude 0 in red, Amplitude 1 in green and Amplitude 2 in blue. Similarly, phase trend image was

25 created by compositing Amplitude 0 in red, Phase 1 in green and Phase 2 in blue. The colors in the amplitude trend and phase trend images can be used as a guide to locating areas that are going through similar trends in seasonality. Furthermore, in order to visualize the changes in seasonality, fitted curves for the beginning and the end

of the series were developed based on the trends determined from the whole series using a Theil–Sen median slope operator.

In order to make the interpretation easier, the seasonal trends were categorized into different classes based on major CMK trend significance. The CMK trend significance for each of the five shape parameters was classified into three major categories: significantly decreasing at the $p < 0.05$ level, not significant, and significantly increasing at the $p < 0.05$ level. All combinations of these significance categories over the trends of five shape parameter (Amplitude 0, Amplitude 1, Amplitude 2, Phase 1 and Phase 2) produced a total of 54 seasonal trend classes. Each class is defined by a combination of five independent tests. Only five major seasonal trend classes in terms of area were selected for detailed analysis.

## 2.6 Change-point analysis

If long-term trends are composed of consecutive segments with gradual change, separated from each other by a relatively short period of abrupt change, such interruptions are referred to as change points or break points (de Jong et al., 2012; Verbesselt et al., 2010). A change-point analysis was conducted, because it indicates that the trends change between positive and negative within the analysis period. Regions of interest (ROIs) were selected for this purpose. The Breaks For Additive Seasonal and Trend (BFAST) method (Verbesselt et al., 2010a, b) and Pettitt test of change-point (Pettitt, 1979) were used to detect and characterize abrupt changes within the trend and seasonal components of the ROI times series. BFAST is an iterative algorithm that integrates the decomposition of time series into seasonal, trend, and remainder component with methods for detecting changes. An additive decomposition model is used to iteratively fit a piecewise linear trend and a seasonal model. The general model is of the form: $Y_t = T_t + S_t + e_t$, $(t \in m)$ where $Y_t$ is the observed NDVI data at time $t$ (in the time series $m$), $T_t$ is the trend component, $S_t$ is the seasonal component, and $e_t$ is the remainder component. A trend component corresponds to a long-term process that operates over the time spanned by the series. A remainder component corresponds to

Full Screen / Esc

Printer-friendly Version

Interactive Discussion

a local process which causes variability between cycles. A seasonal component corresponds to a cyclic process that operates within each cycle.

The other method of change-point detection used in this study is the Pettitt test. The Pettitt test is a nonparametric statistics used to identify a single change point and less sensitive to outliers (Wijngaard et al., 2003). It is extensively employed in change detection studies (Gao et al., 2011; Guerreiro et al., 2014; Villarini et al., 2011).

# 3 Results

## 3.1 Courser scale analysis

### 3.1.1 Inter-annual variability and trends in NDVI in Abay (UBN) basin

The Upper Blue Nile (Abay) basin is characterized by a multi-year mean NDVI of 0.49 for the period 1982–2006 using the GIMMS data set (Fig. 1a). On the one hand, the south and southwest region of the basin represents the highest mean NDVI (Fig. 1a) and the lowest temporal variation (Fig. 1b). This area is characterized by shrubland and woodland vegetation. On the other hand, the eastern, northeastern and northwestern part represents the lowest mean NDVI and the highest temporal variation as a consequence of the relatively low annual precipitation and the more extended dry periods. Besides, this area is characterized by intensive and sedentary cultivation.

During the period 1982–2006, based on median trend about 77 % of the basin showed a positive trend in monthly NDVI with a mean rate of 0.0015 NDVI units (3.77 % yr$^{-1}$) and the remaining 23 % of the basin exhibited a decreasing trend with a mean rate of 0.0007 NDVI units (1.91 % yr$^{-1}$) (Fig. 1a and Table 2). Although the area coverage estimated by the median trend and OLS trend methods are almost similar, the OLS method a little bit underestimates the upward vegetation trend and overestimate the downward vegetation trend. The monthly NDVI increased significantly ($P < 0.05$) over 41.15 % of the basin area, with a mean rate of 0.0023 NDVI units (5.59 % yr$^{-1}$)

and decreased significantly over 4.6 % of the basin, with a mean rate of 0.0017 NDVI units (4.44 % $yr^{-1}$).

Figure 2 depicts the impact of assuming a linear trend development in the 25 years NDVI data series. Figure 2c clearly shows the spatial distribution of the difference between the linear trend and non-linear trend for areas of positive NDVI trend values with mean difference value of 0.043 indicating that the greater part of the basin is described better using a linear trend measure as compared to non-linear trend measure (MK). However, the MK test values in the southern and eastern part of the basin attained higher values as compared to the linear test test. For areas with negative NDVI changes, it appears that the MK test described the NDVI trends better as compared to the LM test with a mean difference value of −0.03 (Fig. 2d).

### 3.1.2 Seasonal trends

More than half (59.52 %) of land areas exhibit a significant trend in seasonality over the 25-year time period measured (1982–2006), producing a total of 53 significantly trending classes of seasonal curves which include different combinations of significant changes in Amplitude 0, Amplitude 1, Amplitude 2, Phase 1 and Phase 2. Thus, a trend change in seasonality is not a rare occurrence in Abay basin. Out of the 53 classes, only the prominent five classes of seasonal trends are described below, which account for about 67 % of all significantly trending pixels and represent 39.95 % of all land pixels of the basin. Eastman et al. (2013) in their global study also found that the trending change in seasonality is not a rare occurrence.

Class 1 has an area of 19 712 $km^2$ which accounts for 16.85 % of all significantly trending areas and 10.03 % of the total land area (Table 3). This class represents areas with a significantly positive trend in Amplitude 0 (mean annual NDVI) and no significant change in any of the other four parameters (Amplitudes, Phases 1 and 2), producing curves that are raised uniformly throughout the year. This implies that an earlier start of green-up, a later start of green-down and an increase in the length of the growing season.

The frequency distribution of seasonal trend classes within zones of land cover types shows that the majority of Class 1 trending pixels occur in areas of woodland (33 %) and shrubland (30 %). Thus, it appears that woodland and shrubland areas are experiencing a consistent increase in productivity throughout the year leading to lengthening of the growing season.

Class 2 is characterized by both a significant increase in Amplitude 0 (mean annual NDVI) and a significant decrease in Phase 1 (orientation with time of the annual cycle). A decreasing phase angle means a shift to a later time of the year. This class has an area of 18 560 km$^2$ and describes about 10 % of the basin land area (Table 3). Figure 4b shows that the green-down period is coming about 15 days later in 2006 than 1982. About 56 % of Class 1 trending pixels occur in areas of woodland. This means that woodland areas of the Upper Blue Nile/Abay basin are experiencing an increase in mean annual NDVI with significant shift in end of growing season and no effect on the start of growing season leading to lengthening of the growing season.

Class 3 represents areas that exhibit a significant increase in Amplitude 1 (the annual cycle), but no other significant trend parameters. Class 3 covers 3.48 % (6848 km$^2$) of all the basin area (Table 3). This class of seasonal trend exhibits a characteristic of increase in NDVI during the growing season (August–November) balanced by declines during the dry season (February–May) in order to maintain the same mean NDVI (Fig. 4c). The majority of Class 3 trending pixels occur in cropland areas (68 % or 4672 km$^2$) of the basin. Therefore, NDVI is enhanced during the green season (cropping season) and inhibited during the brown season or harvest.

Class 4 represents areas that exhibit a significant decrease in Amplitude 1 (the annual cycle), but no other significant trend parameters. Class 4 covers 9.51 % (18 688 km$^2$) of all the basin area (Table 3). This class of seasonal trend exhibits a characteristic decrease in NDVI during the growing season (more pronounced between August–November) increase in NDVI during dry season (Fig. 4d). Class 4 seasonal trend pixels are mostly associated with cropland (59 %) and grassland (19 %) land

cover types. This type of seasonal trend is more common in North Gojam and Lake Tana sub-basins.

Class 5 describes areas that show a significant decrease in Phase 1 only. Class 5 seasonal curves resemble Class 2 seasonal curves in that both have similar pattern of a decrease in yearly phase. It covers 7.5 % (14 720 km$^2$) of all the basin area and represents 12.6 % of all significant seasonal trend pixels. This class of seasonal trend exhibits a characteristic shift in the end of growing season. Class 5 pixels are mostly associated with woodland (48 %) and cropland (30 %). This type of seasonal trend is more common in southern and southwestern part of the basin.

All except Class 4 showed a general increase in length of growing season and this class is mainly found in woodland and shrubland areas. Thus, it appears that woodland and shrubland areas are experiencing a consistent increase in productivity throughout the year leading to lengthening of the growing season.

### 3.1.3  Trend break analysis

**Trend break analysis in the inter-annual data series**

The tread break analysis of ROIs shown in Fig. 5 illustrates different trend behavior within a longer time series of satellite data. Trends are not always continuously increasing or decreasing but can change over time. For example, ROI #2 (Fig. 5b) and ROI #4 (Fig. 5d) represent gradual browning and greening trends, respectively, over the entire study period, while ROI #1 and ROI #3 describe abrupt browning and greening, respectively. ROI #1 characterized by trend breaks at December 1989 and August 1997 and ROI #3 shows a trend break at April 1998. Thus, the trend break analysis assisted identification of several change periods which might otherwise been overlooked through a commonly assumed fixed change trajectory analysis.

It is beyond the capacity of this study to interpret driving factors behind the observed vegetation changes, but literature suggests that the most likely driving factor of monotonic greening or browning as observed in ROI #2 and ROI #4 could be changes

in growth-limiting climatologies (Nemani et al., 2003), broad-scale land management practices, and persistent land use change driven by settlements (e.g. cropland expansion and urbanization) (Ramankutty et al., 2007). Strongest indication for greening in agricultural expansion areas such as Fincha and Belles sub-basins is most likely attributable to improved agricultural techniques. Abrupt browning as observed in ROI #1 could be caused by logging followed by regrowth or the already existed vegetation decline in some places might have amplified by to a period of persistently poor rains. However, abrupt greening as observed in ROI #3 could be caused by wet period induced by El Niño/La Niña Southern Oscillation (ENSO) warming events such as ENSO 1986/87, 1994/95, and 1997/98. Thus, greening might represent recovery from drought or other disturbances such as forest fire (Anyamba and Tucker, 2005; Olsson et al., 2005). Finally, although the GIMMS data sets have been thoroughly corrected (Tucker et al., 2005), AVHRR satellite platform changes could potentially cause trend breaks within the time series. The detected trend break time was compared with the time of AVHRR platform change (1985, 1988, 1994, 1995, 2000 and 2004) and it was found that that they are different.

**Trend break analysis in the HANTS seasonality parameters**

Trend break analysis was performed to identify times when abrupt changes within the trends of harmonic series shape parameters occurred. The Pettitt test change point analysis for Class 1 shows that there is a significant shift ($k = 117$, $p = 0.001$) between two parts of the NDVI time series at the year 1998 (Fig. 6). The mean annual NDVI (A0) increased from a mean of 0.48 NDVI units observed for the period 1982–1998 to a mean value of 0.51 NDVI units observed for the period 1999–2006. A significant decreasing shift of Phase 1 occurred at the year 1997 for class 2 seasonal trend class (i.e. mainly woodland) from a mean phase angle of 217° observed during 1982–1997 to a mean phase angle of 210° during 1998–2006. This means the green-down period shifts to a later time of the year which has also implication on increasing length of

growing season since 1998. Figure 6 also shows a significant increasing shift ($k = 124$, $p = 0.001$) of the annual amplitude from 0.15 to 0.17 NDVI units at the year 1998.

## 3.2 Fine scale vegetation tend analysis

### 3.2.1 Inter-annual trend analysis

Figure 7a shows that areas of higher multi-year mean NDVI depict lower vegetation cover variability (Fig. 7b). Areas located in the eastern part of the basin are those with higher variability and show an upward (positive) trend of vegetation growth in the period 2001–2011 (Fig. 7b and c). About 36 % of the UBN/Abay basin shows a significantly browning trend ($P < 0.05$) over the period 2001–2011 at an average rate of 0.0768 NDVI yr$^{-1}$ using MODIS 250 m spatial resolution (Tables 4 and 5). By contrast, only about 1.19 % of the basin shows a significantly greening trend ($P < 0.05$) over the period 2001–2011 at an average rate of 0.066 NDVI yr$^{-1}$ (Tables 4 and 5). The majority of this browning trend comes from Dabus (14.27 % at a rate of 0.0744), Belles (13.5 % at a rate of 0.0816), Wonbera (11.81 % at a rate of 0.0792) and Didessa (11.48 % at a rate of 0.0792). The vegetation activity in Belles sub basin is being decreased at a faster rate (0.0816 NDVI yr$^{-1}$) than the others (Tables 4 and 5).

The Maximum significant browning slope observed in Didessa sub-basin is the largest of all maximum slopes in the basin. The size of greening and the browning area within sub-basins are proportional in sub-basins such as Beshillo, Jemma, Muger and Welaka. Whereas, more than half of the areas of the Belles (66.91 %), Rahad (60.41 %), and Wonbera (64. 12%) are represented by significant browning trend. The majority of this greening trend comes from Jemma (22.03 % at a rate of 0.066), Beshillo (18.23 % at a rate of 0.066), North Gojam (22.78 % at a rate of 0.066), and Muger (12.15 % at a rate of 0.0648) sub-basins. The slowest rate and the fastest rate of significant greening are observed in Dinder sub-basin (0.0552 NDVI yr$^{-1}$) and Dabus sub-basin (0.0768 NDVI yr$^{-1}$), respectively.

### 3.2.2 Intra-annual trends

About 207 classes of significant intra-annual changes (prominent classes are depicted in Fig. 8a), that include different combinations of significant changes in Amplitude 0, Amplitude 1, Amplitude 2, Phase 1 and 2, were found. The fine scale analysis revealed that about 96 % of the basin represents significant seasonal trends, out of which 33.15 % represents the dominant classes. About 46 % of the dominant classes represent areas with vegetation that underwent significant decrease in the annual vegetation cycle (A1) or both the annual vegetation cycle (A1) and mean annual vegetation cycle (A0) (Fig. 8a). These areas are represented by ROI#2, ROI#5 and ROI#8 (Fig. 8a and b). Figure 9b and e show a change in the greenness pattern from a strong mean annual and annual cycle of these areas to strong semi-annual vegetation cycle. This change was found to be statistically significant ($P < 0.05$) based on the CMK test. This means these areas underwent significant changes from shrubland/woodland vegetation to double cropping (irrigation) during the period 2001–2011. For example, ROI#2 and ROI#5 located in the light green color of Fig. 8a represents small-scale irrigation areas with strong semi-annual cycle in Didessa sub-basins. Similarly, the blue color in Fig. 8b is also dominant in the Belles sub-basin (ROI#8), which indicates the vegetation in this area has changed from strong annual mean and annual NDVI to a strong semi-annual vegetation cycle. This is a typical characteristic of change in land use from shrubs and bushes to irrigated cropland.

The Magenta color is dominant in Muger (ROI#1), Guder and North Gojam sub-basins and it represents a significant change from strong annual vegetation cycle to strong mean annual and semi-annual vegetation cycles. The western part of the basin is dominated by yellow color (ROI#6), which means that the cycle of vegetation has undergone a change from strong semi-annual to strong mean annual. Cyan color is wide spread, particularly in Didessa sub-basin (ROI#3), meaning that currently the vegetation in this area is characterized by a significant decrease in mean annual vegetation cycle indicating degradation of forest without complete removal. Figure 9c shows a de-

crease in vegetation condition in the sampled area, while the NDVI still remain above 0.8.

The UBN/Abay basin is not only characterized by a significant decreasing seasonal trend of vegetation but also increasing trend. The increasing seasonal trends are mostly found, in the eastern part of the basin, where previous de-vegetation took place. For example, the Jema (ROI#7) sub-basin is one of the areas that a significantly increasing mean annual NDVI can be observed. In other words, there has been a change from a strong semi-annual vegetation cycle to strong mean annual NDVI. This could be related to increased vegetation activity in the area (e.g. on-farm eucalyptus plantation). ROI#4 is also another example for a significant increasing trend. ROI#4 represents a significant change from strong annual vegetation cycle to strong mean annual and semi-annual vegetation cycles. This is due to small-scale irrigation development on the area mainly because of the change in river course of Megech, North of Lake Tana.

### 3.2.3 Change point analysis of MODIS NDVI (2001–2011)

The trend break analysis performed using the BFAST approach was not able to detect trend breaks in all of the sampled areas (Fig. 10) suggesting that vegetation activity in Abay basin showed a monotonic increasing or decreasing behavior, even if trend shifts are accounted for. Slowly acting processes such as land management practices or land degradation may cause such monotonic changes in the time series. Only ROI#4 shows a significant shift in the seasonal component at 2008 in Fig. 10c and the break point indicates the start of double cropping in the area. However, the Pettitt's test identified different significant shifts at specific points in time for the three amplitude components. Table 6 shows the Pettitt's test result for identifying the time at which the shift occurs. The downward shift occurred during the period 2004–2006. For example, a highly significant ($P < 0.01$) decreasing shift in A0 occurred in 2004 for ROI#2 and in 2005 for ROI#5 and ROI#8. A highly significant ($P < 0.01$) decreasing shift in A1 occurred in 2006 for ROI#2 and 2005 for ROI#8. Thus, the significant decreasing shift in the veg-

etation condition of Abay basin occurred mainly during the period 2004–2006. This indicates a recent decline in vegetation activity.

Significant increasing shift in the MODIS annual mean NDVI (A0) was observed in ROI#4 in 2007 ($P < 0.05$) and in ROI#7 in 2004 ($P < 0.01$) (Table 6). Annual amplitude also showed a significant increase in 2007 in ROI#4 ($P < 0.1$). Thus, 2007 can be considered as the time when a significant increase in vegetation condition occurred.

## 4 Discussion

### 4.1 Course scale analysis

The courser scale vegetation trend analysis using the monthly GIMMS NDVI revealed a significant increase in the vegetation condition over 41.15 % of the Abay basin for the period 1982–2006. Several studies have also reported widespread greening and increased vegetation growth and productivity for various areas of the world particularly in the Northern Hemisphere (Nemani et al., 2003; Slayback et al., 2003; Zhou et al., 2001). The north western and western parts of the basin that exhibited positive NDVI change are mainly covered with lowland vegetation such as woodland and shrubland. These areas are used for traditional uses such as shifting cultivation and livestock rearing, by the small indigenous population. One key characteristic of these areas is the periodic burning of vegetation, as it is evident from fire scares visible on Landsat images. The reason for this burning is not clear. Thus, the positive NDVI trend of these areas could be attributed to a decreasing trend of burning of vegetation. However, detailed investigation of these areas is crucial to be able to attribute the trend to particular cause.

The basin is characterized not only by significant inter-annual variation, but also by a significant trend in seasonality. More than half (59.52 %) of land areas exhibited a significant trend in seasonality over the 25-year time period measured (1982–2006). Thus, a trend in seasonality is not a rare occurrence in Abay basin. Eastman et al. (2013) in

their global study also concluded that a significant trend in seasonality is not a rare occurrence. Areas with significantly positive trend in mean annual NDVI (Amplitude 0) were found to be the dominant seasonal trend class, which accounts for 16.85 % of all significantly trending areas and 10.03 % of the total land area. The majority of this seasonal trend class occurs in areas of woodland and shrubland. A significant increase in mean annual NDVI without significant changes in any of the other harmonic shape parameters implies lengthening of the growing season. This result is consistent with a myriad of previous findings from both station observations and satellite observations. Studies in the Northern Hemisphere using phenology and temperature observations from stations have reported an increase in plant growth associated with a lengthening of the growing season (Menzel et al., 2006; Sparks et al., 2009). Findings from analysis of satellite observations (Karlsen et al., 2007; Tucker et al., 2001; Zhou et al., 2001) also supported the results of station observations. A longer growing season could bring an increased photosynthesis by plants (Richardson et al., 2010) and it correlates strongly with annual gross primary productivity (Reed et al., 1994). Thus, it appears that woodland and shrubland areas of Abay basin are experiencing a consistent increase in productivity throughout the year.

It is beyond the capacity of this study to interpret driving factors behind the observed vegetation changes, but literature suggested that the most likely driving factor of monotonic greening or browning could be changes in growth-limiting climatologies (Nemani et al., 2003), broad-scale land management practices, and persistent land use change driven by settlements (e.g. cropland expansion and urbanization) (Ramankutty et al., 2007). Strongest indication for greening in agricultural expansion areas such as Fincha and Belles sub-basins is most likely attributable to improved agricultural techniques. Abrupt browning could be caused by logging followed by regrowth or the already existed vegetation decline in some places might have amplified by to a period of persistently poor rains. However, abrupt greening could be caused by wet period induced by El Niño/La Niña Southern Oscillation (ENSO) warming events such as ENSO 1986/87, 1994/95, and 1997/98. The year 1997/1998 was identified as a trend

break point using the Pettitt test. Thus, greening might represent recovery from drought or other disturbances such as forest fire (Anyamba and Tucker, 2005; Heumann et al., 2007; Olsson et al., 2005). Finally, although the GIMMS data sets have been thoroughly corrected (Tucker et al., 2005), AVHRR satellite platform changes could potentially cause trend breaks within the time series. The detected trend break time was compared with the time of AVHRR platform change (1985, 1988, 1994, 1995, 2000 and 2004) (Tucker et al., 2005) and it was found that that they are different. With regard to attribution of vegetation trend to the drivers, the courser scale analysis only provides indications for more focused analysis, because the driving factors might act on a local scale much smaller than the resolution of GIMMS NDVI (i.e. 8 km). Thus, based on the information obtained from this courser scale analysis area specific attribution of the increase in greenness to its causes is required for the Abay basin for the future.

## 4.2 Fine scale analysis

The vegetation trend analysis with a spatial resolution of 250 m MODIS (2001–2011) depicted a different perspective from that of 8 km spatial resolution of GIMMS data set (1982–2006). About 36 % of the UBN/Abay basin showed a significantly browning trend and only 1.19 % of the basin showed a significantly greening trend over the period 2001–2011. The majority of the browning trend comes from Dabus, Belles, Wonbera and Didessa. The fine scale vegetation seasonal trend analysis during the period 2001–2011 revealed three conspicuous vegetation changes: (1) a change in the greenness pattern from a strong mean annual and annual cycle to strong semi-annual vegetation cycle, indicating significant changes from shrubland/woodland vegetation to double cropping (irrigation) (e.g. ROI#2, ROI#5 and ROI#8); (2) degradation of vegetation without complete removal (e.g. ROI#3); and (3) a change from a strong semi-annual vegetation cycle to strong mean annual NDVI, which could be related to increased vegetation activity in the area (e.g. on-farm eucalyptus plantation). These areas could have been masked if only the inter-annual vegetation trend analysis was performed. Thus, carrying out intra-annual trend analysis would be helpful especially in fine scale

analysis since most of the deforestations for the purpose of small scale irrigation are operating at local scale.

Although the BFAST approach of the trend break analysis indicated a monotonic increasing or decreasing vegetation condition without any significant trend breaks. However, based on Pettitt's test, it was possible to detect trend shifts for different HANTS shape parameters. The significant decreasing shift in the vegetation condition of Abay basin occurred mainly during the period 2004–2006. The greening tend observed from GIMMS data set might have been reversed into browning trend suggesting a localized decline in vegetation activity during the period 2004–2006. This result is consistent with the findings of de Jong et al. (2013), who explained a trend reversal into browning trend not confined to single geographical region, but extended across all continents. In the 1980s and 1990s the Northern Hemisphere was found to become greener (Nemani et al., 2003; Zhou et al., 2001). Some anthropogenic factors could be attributed to the observed recent browning trend in the basin. One of the possible drivers of browning in the northwest part of the basin especially in Rahad and some part Dinder sub-basins could be intra-regional resettlement (i.e. people from the same area with kin relations in the same locality) and its associated deforestation for cropland expansion (Dixon and Wood, 2007; Lemenih et al., 2014). The Amhara regional government of Ethiopia initiated "voluntary" resettlement scheme since 2003 for the most chronically food insecure people from all zones of the region to potentially more productive, fertile and less populated parts such as Metema, Quara, Tach Armacheho and Tegede woredas of North Gondar administrative zone (NCFSE, 2003). In the Belles sub-basin land preparation for small to medium scale irrigation schemes could initially cause a decline in vegetation trend, but after a while the browning trend might be reversed to greening trend. Currently, private and government agricultural investments are underway in this sub-basin. Thus, the decreasing trend of vegetation greenness in the Belles sub-basin can be largely explained by the de-vegetation during land preparation for sugarcane plantation particularly in Alefa and Jawi weredas from Amhara regional state and Pawe and Dandur weredas from Benshagul Gumz regional states of Ethiopia. Such big crop-

lands could contribute to the browning in the initial stage and to the greening once the cropland is established.

## 5 Conclusions

There are two notable features of long-term trend analysis conducted on monthly GIMMS NDVI data from 1982 to 2006. First, based on robust trend estimators (Theil–Sen slope) most part of the Upper Blue Nile basin ($\sim 77\%$) showed a positive trend in monthly NDVI with a mean rate of 0.0015 NDVI units ($3.77\% \, \mathrm{yr}^{-1}$), out of which 41.15 % of the basin area depicted significant increases ($P < 0.05$) with a mean rate of 0.0023 NDVI units ($5.59\% \, \mathrm{yr}^{-1}$). Second, the upward trend (positive change) in NDVI is most intense in the northwestern and downward trend (negative change) in NDVI is intense in the southern and eastern part of the basin. Areas showing high NDVI variability were found to be the ones exhibiting long-term positive trends. The fine scale (250 m) MODIS-based vegetation trend analysis revealed that about 36 % of the UBN/Abay basin shows a significantly browning trend ($P < 0.05$) over the period 2001–2011 at an average rate of $0.0768 \, \mathrm{NDVI} \, \mathrm{yr}^{-1}$ using MODIS 250 m spatial resolution. The majority of this browning trend comes from the sub-basins Dabus, Belles, Wonbe, and Didessa. The vegetation activity in the Belles sub basin has decreased at a faster rate ($0.082 \, \mathrm{NDVI} \, \mathrm{yr}^{-1}$) than the other sub-basins. The greening trend observed from the GIMMS data set might have been reversed into browning trend and suggests a localized decline in vegetation activity in recent years. Anthropogenic factors such as resettlement and agricultural expansion could be attributed to the observed greening-to-browning reversal of vegetation conditions in the UBN basin.

Intra-annual trend analysis identified changes in vegetation condition that could have been masked if only the inter-annual vegetation trend analysis was performed. Changes in seasonality was found to be prevalent in the landscape of Upper Blue Nile/Abay basin as more than half (59.52 %) of land areas exhibit a significant trend in seasonality over the 25-year time period measured (1982–2006). Only five types of

seasonal trends were dominant out of which the largest proportion describes areas that are experiencing a uniform increase in NDVI throughout the year. It appears that woodland and shrubland areas of the basin experienced increase in vegetation pro-ductivity resulting from longer growing season. The fine scale seasonal trend analysis of MODIS NDVI (2001–2011) also confirmed that seasonal trend is not a rare occur-rence in the Abay basin as 96 % of the basin represents significant seasonal trends. Moreover, it revealed three conspicuous vegetation changes: (1) significant changes from shrubland/woodland vegetation to double cropping (irrigation); (2) degradation of vegetation without complete removal; and (3) localized increased vegetation activity.

Trend break analysis of GIMMS NDVI (1982–2006) showed that trends in vegetation conditions of the UBN basin were found to be not only monotonic, but also abrupt. The step change was detected in 1997/1998 in both inter-annual and intra-annual veg-etation time series analysis. Thus, the trend break analysis assisted identification of several change periods which might otherwise be overlooked through a commonly as-sumed fixed change trajectory analysis. On the other hand, the trend break analysis performed on MODIS NDVI (2001–2011) using BFAST approach were not able to de-tect trend breaks suggesting that vegetation activity in Abay basin showed a monotonic increasing or decreasing behavior. Slowly acting processes such as land management practices or land degradation may cause such monotonic changes in the time series. However, the Pettitt test identified the significant decreasing shift in the vegetation con-dition of the Abay basin occurred mainly during the period 2004–2006. This indicates a recent decline in vegetation activity.

This study concludes that integrated analysis of course and fine scale, inter-annual and intra-annual trend revealed the following points:

– The greening trend of vegetation condition was followed by browning trend since mid-2000s in the Abay basin. Thus, there is an urgent need in increasing the vegetation activities in the basin.

- Intra-annual trend analysis was found to be very useful in identifying changes in vegetation condition that could have been masked if only the inter-annual vegetation trend analysis was performed.

- The finer scale intra-annual trend analysis revealed trends that were more linked to human activities;

# References

Angert, A., Biraud, S., Bonfils, C., Henning, C., Buermann, W., Pinzon, J., Tucker, C., and Fung, I.: Drier summers cancel out the $CO_2$ uptake enhancement induced by warmer springs, P. Natl. Acad. Sci. USA, 102, 10823–10827, 2005.

Anyamba, A. and Tucker, C.: Analysis of Sahelian vegetation dynamics using NOAA-AVHRR NDVI data from 1981–2003, J. Arid Environ., 63, 596–614, 2005.

Bai, Z. G., Dent, D. L., Olsson, L., and Schaepman, M. E.: Proxy global assessment of land degradation, Soil Use Manage., 24, 223–234, 2008.

Bala, G., Joshi, J., Chaturvedi, R. K., Gangamani, H. V., Hashimoto, H., and Nemani, R.: Trends and variability of AVHRR-derived NPP in India, Remote Sens., 5, 810–829, 2013.

Baldocchi, D., Falge, E., Gu, L., Olson, R., Hollinger, D., Running, S., Anthoni, P., Bernhofer, C., Davis, K., and Evans, R.: FLUXNET: A new tool to study the temporal and spatial variability of ecosystem-scale carbon dioxide, water vapor, and energy flux densities, B. Am. Meteorol. Soc., 82, 2415–2434, 2001.

Buenemann, M., Martius, C., Jones, J., Herrmann, S., Klein, D., Mulligan, M., Reed, M., Winslow, M., Washington-Allen, R., and Lal, R.: Integrative geospatial approaches for the comprehensive monitoring and assessment of land management sustainability: rationale, potentials, and characteristics, Land Degrad. Dev., 22, 226–239, 2011.

De Beurs, K., Wright, C., and Henebry, G.: Dual scale trend analysis for evaluating climatic and anthropogenic effects on the vegetated land surface in Russia and Kazakhstan, Environ. Res. Lett., 4, 045012, doi:10.1088/1748-9326/4/4/045012, 2009.

de Jong, R., de Bruin, S., de Wit, A., Schaepman, M. E., and Dent, D. L.: Analysis of monotonic greening and browning trends from global NDVI time-series, Remote Sens. Environ., 115, 692–702, 2011.

de Jong, R., Verbesselt, J., Schaepman, M. E., and Bruin, S.: Trend changes in global greening and browning: contribution of short-term trends to longer-term change, Glob. Change Biol., 18, 642–655, 2012.

de Jong, R., Verbesselt, J., Zeileis, A., and Schaepman, M. E.: Shifts in global vegetation activity trends, Remote Sens., 5, 1117–1133, 2013.

De Wit, A. and Su, B.: Deriving phenological indicators from SPOT-VGT data using the HANTS algorithm, 2nd international SPOT-VEGETATION user conference, Antwerp, Belgium, 195–201, 2005.

Dixon, A. B. and Wood, A. P.: Local institutions for wetland management in Ethiopia: Sustainability and state intervention, Community-based water law and water resource management reform in developing countries, 130–145, 2007.

Dregne, H., Kassas, M., and Rozanov, B.: A new assessment of the world status of desertification, Desertification Control Bulletin, 20, 6–18, 1991.

Eastman, J. R., Sangermano, F., Machado, E. A., Rogan, J., and Anyamba, A.: Global trends in seasonality of normalized difference vegetation index (NDVI), 1982–2011, Remote Sens., 5, 4799–4818, 2013.

Fensholt, R., Rasmussen, K., Nielsen, T. T., and Mbow, C.: Evaluation of earth observation based long term vegetation trends – Intercomparing NDVI time series trend analysis consistency of Sahel from AVHRR GIMMS, Terra MODIS and SPOT VGT data, Remote Sens. Environ., 113, 1886–1898, 2009.

Gallo, K., Ji, L., Reed, B., Eidenshink, J., and Dwyer, J.: Multi-platform comparisons of MODIS and AVHRR normalized difference vegetation index data, Remote Sens. Environ., 99, 221–231, 2005.

Gao, P., Mu, X.-M., Wang, F., and Li, R.: Changes in streamflow and sediment discharge and the response to human activities in the middle reaches of the Yellow River, Hydrol. Earth Syst. Sci., 15, 1–10, doi:10.5194/hess-15-1-2011, 2011.

Title Page

Abstract | Introduction

Conclusions | References

Tables | Figures

|◄ | ►|

◄ | ►

Back | Close

Full Screen / Esc

Printer-friendly Version

Interactive Discussion

Gilbert, R. O.: Statistical methods for environmental pollution monitoring, John Wiley & Sons, Pacific Northwest Lab., Richland, WA, USA, 1987.

Godfray, H. C. J., Beddington, J. R., Crute, I. R., Haddad, L., Lawrence, D., Muir, J. F., Pretty, J., Robinson, S., Thomas, S. M., and Toulmin, C.: Food security: the challenge of feeding 9 billion people, Science, 327, 812–818, 2010.

Guerreiro, S. B., Kilsby, C. G., and Serinaldi, F.: Analysis of time variation of rainfall in transnational basins in Iberia: abrupt changes or trends?, Int. J. Climatol., 34, 114–133, 2014.

Harris, I., Jones, P., Osborn, T., and Lister, D.: Updated high-resolution grids of monthly climatic observations–the CRU TS3. 10 Dataset, Int. J. Climatol., 34, 623–642, 2014.

Harris, J. W. and Stöcker, H.: Handbook of mathematics and computational science, Springer, New York, USA, ISBN: 0387947469, 9780387947464, 1028 pp., 1998.

Henebry, G. M.: Global change: carbon in idle croplands, Nature, 457, 1089–1090, 2009.

Heumann, B. W., Seaquist, J., Eklundh, L., and Jönsson, P.: AVHRR derived phenological change in the Sahel and Soudan, Africa, 1982–2005, Remote Sens. Environ., 108, 385–392, 2007.

Hoaglin, D. C., Mosteller, F., and Tukey, J. W.: Understanding robust and exploratory data analysis, Wiley New York, 1983.

Holben, B. N.: Characteristics of maximum-value composite images from temporal AVHRR data, Int. J. Remote Sens., 7, 1417–1434, 1986.

Huete, A., Didan, K., Miura, T., Rodriguez, E. P., Gao, X., and Ferreira, L. G.: Overview of the radiometric and biophysical performance of the MODIS vegetation indices, Remote Sens. Environ., 83, 195–213, 2002.

Jakubauskas, M. E., Legates, D. R., and Kastens, J. H.: Harmonic analysis of time-series AVHRR NDVI data, Photogramm. Eng. Rem. S., 67, 461–470, 2001.

Karlsen, S. R., Solheim, I., Beck, P. S., Høgda, K. A., Wielgolaski, F. E., and Tømmervik, H.: Variability of the start of the growing season in Fennoscandia, 1982–2002, Int. J. Biometeorol., 51, 513–524, 2007.

Kearney, J.: Food consumption trends and drivers, Philos. T. Roy. Soc. B, 365, 2793–2807, 2010.

Kendall, M. G.: Rank correlation methods, Hafner, New York, 1948.

Landin, M. G. and Bosart, L. F.: The diurnal variation of precipitation in California and Nevada, Mon. Weather Rev., 117, 1801–1816, 1989.

Inter-annual and seasonal trends of vegetation

E. Teferi et al.

Title Page

Abstract | Introduction

Conclusions | References

Tables | Figures

|◄ | ►|

◄ | ►

Back | Close

Full Screen / Esc

Printer-friendly Version

Interactive Discussion

Legates, D. R. and Willmott, C. J.: Mean seasonal and spatial variability in gauge-corrected, global precipitation, Int. J. Climatol., 10, 111–127, 1990.

Lemenih, M., Kassa, H., Kassie, G. T., Abebaw, D., and Teka, W.: Resettlement and wood-land management problems and options: a case study from North-western Ethiopia, Land Degrad. Dev., 25, 305-318, 2014

Madden, R. A. and Julian, P. R.: Detection of a 40–50 day oscillation in the zonal wind in the tropical Pacific, J. Atmos. Sci., 28, 702–708, 1971.

Mann, H. B.: Nonparametric tests against trend, Econometrica: Journal of the Econometric Society, 13, 245–259, 1945.

Menzel, A., Sparks, T. H., Estrella, N., Koch, E., Aasa, A., Ahas, R., Alm-Kübler, K., Bissolli, P., Braslavská, O. G., and Briede, A.: European phenological response to climate change matches the warming pattern, Glob. Change Biol., 12, 1969–1976, 2006.

Metternicht, G., Zinck, J., Blanco, P., and Del Valle, H.: Remote sensing of land degradation: Experiences from Latin America and the Caribbean, J. Environ. Qual., 39, 42–61, 2010.

Nagol, J. R., Vermote, E. F., and Prince, S. D.: Effects of atmospheric variation on AVHRR NDVI data, Remote Sens. Environ., 113, 392–397, 2009.

NCFSE: Voluntary Resettlement Programme (Access to improved land), Vol. II, Addis Ababa, Ethiopia, 2003.

Neeti, N. and Eastman, J. R.: A contextual mann-kendall approach for the assessment of trend significance in image time series, Transactions in GIS, 15, 599–611, 2011.

Nemani, R. R., Keeling, C. D., Hashimoto, H., Jolly, W. M., Piper, S. C., Tucker, C. J., Myneni, R. B., and Running, S. W.: Climate-driven increases in global terrestrial net primary production from 1982 to 1999, Science, 300, 1560–1563, 2003.

Olsson, L., Eklundh, L., and Ardö, J.: A recent greening of the Sahel – trends, patterns and potential causes, J. Arid. Environ., 63, 556–566, 2005.

Pettitt, A.: A non-parametric approach to the change-point problem, Applied statistics, 28, 126–135, 1979.

Ramankutty, N., Gibbs, H. K., Achard, F., Defries, R., Foley, J. A., and Houghton, R.: Challenges to estimating carbon emissions from tropical deforestation, Glob. Change. Biol., 13, 51–66, 2007.

Reed, B. C., Brown, J. F., VanderZee, D., Loveland, T. R., Merchant, J. W., and Ohlen, D. O.: Measuring phenological variability from satellite imagery, J. Veg. Sci., 5, 703–714, 1994.

Richardson, A. D., Black, T. A., Ciais, P., Delbart, N., Friedl, M. A., Gobron, N., Hollinger, D. Y., Kutsch, W. L., Longdoz, B., and Luyssaert, S.: Influence of spring and autumn phenological transitions on forest ecosystem productivity, Philos. T. Roy. Soc. B., 365, 3227–3246, 2010.

Roerink, G., Menenti, M., and Verhoef, W.: Reconstructing cloudfree NDVI composites using Fourier analysis of time series, Int. J. Remote Sens., 21, 1911–1917, 2000.

Sen, P. K.: Estimates of the regression coefficient based on Kendall's tau, J. Am. Stat. Assoc., 63, 1379–1389, 1968.

Slayback, D. A., Pinzon, J. E., Los, S. O., and Tucker, C. J.: Northern hemisphere photosynthetic trends 1982–99, Glob. Change Biol., 9, 1–15, 2003.

Sparks, T. H., Menzel, A., and Stenseth, N. C.: European cooperation in plant phenology, Clim. Res., 39, 175–177, 2009.

Thiel, H.: A rank-invariant method of linear and polynomial regression analysis, Part 3, Proceedings of Koninalijke Nederlandse Akademie van Weinenschatpen A, 1397–1412, 1950.

Townshend, J. R. and Justice, C. O.: Selecting the spatial resolution of satellite sensors required for global monitoring of land transformations, Int. J. Remote Sens., 9, 187–236, 1988.

Tucker, C. J., Slayback, D. A., Pinzon, J. E., Los, S. O., Myneni, R. B., and Taylor, M. G.: Higher northern latitude normalized difference vegetation index and growing season trends from 1982 to 1999, Int. J. Biometeorol., 45, 184–190, 2001.

Tucker, C. J., Pinzon, J. E., Brown, M. E., Slayback, D. A., Pak, E. W., Mahoney, R., Vermote, E. F., and El Saleous, N.: An extended AVHRR 8 km NDVI dataset compatible with MODIS and SPOT vegetation NDVI data, Int. J. Remote Sens., 26, 4485–4498, 2005.

UNEP: Global Environmental Outlook, New York, October, 2007.

Verbesselt, J., Hyndman, R., Newnham, G., and Culvenor, D.: Detecting trend and seasonal changes in satellite image time series, Remote Sens. Environ., 114, 106–115, 2010a.

Verbesselt, J., Hyndman, R., Zeileis, A., and Culvenor, D.: Phenological change detection while accounting for abrupt and gradual trends in satellite image time series, Remote Sens. Environ., 114, 2970–2980, 2010b.

Verhoef, A., van den Hurk, B. J., Jacobs, A. F., and Heusinkveld, B. G.: Thermal soil properties for vineyard (EFEDA-I) and savanna (HAPEX-Sahel) sites, Agr. Forest Meteorol., 78, 1–18, 1996.

Villarini, G., Smith, J. A., Baeck, M. L., Vitolo, R., Stephenson, D. B., and Krajewski, W. F.: On the frequency of heavy rainfall for the Midwest of the United States, J. Hydrol., 400, 103–120, 2011.

Title Page

Abstract | Introduction

Conclusions | References

Tables | Figures

|◄ | ►|

◄ | ►

Back | Close

Full Screen / Esc

Printer-friendly Version

Interactive Discussion

Vogt, J., Safriel, U., Von Maltitz, G., Sokona, Y., Zougmore, R., Bastin, G., and Hill, J.: Monitoring and assessment of land degradation and desertification: Towards new conceptual and integrated approaches, Land Degrad. Dev., 22, 150–165, 2011.

Vuichard, N., Ciais, P., Belelli, L., Smith, P., and Valentini, R.: Carbon sequestration due to the abandonment of agriculture in the former USSR since 1990, Global Biogeochem. Cy., 22, doi:10.1029/2008GB003212, 2008.

Wang, X. L. and Swail, V. R.: Changes of extreme wave heights in Northern Hemisphere oceans and related atmospheric circulation regimes, J. Climate, 14, 2204–2221, 2001.

Wessels, K., Prince, S., Frost, P., and Van Zyl, D.: Assessing the effects of human-induced land degradation in the former homelands of northern South Africa with a 1 km AVHRR NDVI time-series, Remote Sens. Environ., 91, 47–67, 2004.

Wessels, K., Prince, S., Malherbe, J., Small, J., Frost, P., and VanZyl, D.: Can human-induced land degradation be distinguished from the effects of rainfall variability? A case study in South Africa, J. Arid Environ., 68, 271–297, 2007.

Wijngaard, J., Klein Tank, A., and Können, G.: Homogeneity of 20th century European daily temperature and precipitation series, Int. J. Climatol., 23, 679–692, 2003.

Wilks, D. S.: Statistical methods in the atmospheric sciences, Academic press, USA, 2011.

Zhao, M. and Running, S. W.: Drought-induced reduction in global terrestrial net primary production from 2000 through 2009, Science, 329, 940–943, 2010.

Zhou, L., Tucker, C. J., Kaufmann, R. K., Slayback, D., Shabanov, N. V., and Myneni, R. B.: Variations in northern vegetation activity inferred from satellite data of vegetation index during 1981 to 1999, J. Geophys. Res.-Atmos., 106, 20069–20083, 2001.

Title Page

Abstract | Introduction

Conclusions | References

Tables | Figures

Back | Close

Full Screen / Esc

Printer-friendly Version

Interactive Discussion

**Table 1.** Parameters used in HANTS analysis.

| HANTS parameters | GIMMS | | MODIS | |
|---|---|---|---|---|
| | Single year | Full data set | Single year | Full data set |
| Number of frequency | 0, 1, 2 | 0, 24, 48 | 0, 1, 2 | 0, 23, 46 |
| Invalid data rejection threshold: | 0–1 | 0–1 | 0–1 | 0–1 |
| Fit error tolerance (FET) | 0.1 | 0.1 | 0.1 | 0.1 |
| Maximum iterations ($i_{MAX}$) | 6 | 12 | 6 | 12 |
| Minimum retained data points | 16 | 416 | 15 | 165 |

**Table 2.** Trend analysis result for the monthly GIMMS NDVI data.

| Trend estimators | Trend estimator | Slope | | MK-Z trends | |
|---|---|---|---|---|---|
| | | Positive | Negative | Significantly + | Significantly − |
| Ordinary least square (OLS) slope | ΔNDVI/month | 0.0015 | 0.008 | 0.0023 | 0.0019 |
| | % NDVI change/month | 0.317 | 0.189 | 0.464 | 0.428 |
| | Land area (%) | 75.06 | 24.94 | 41.15 | 4.60 |
| Theil–Sen(TS) (median) slope | ΔNDVI/month | 0.0015 | 0.0007 | 0.0023 | 0.0017 |
| | % NDVI change/month | 0.314 | 0.159 | 0.466 | 0.370 |
| | Land area (%) | 76.85 | 23.15 | 41.15 | 4.60 |

**Table 3.** The most important land cover classes for each major significant seasonal trend categories.

| Classes of seasonal trends | Grassland | Shrubland | Woodland | Bare land | Crop land | Natural Forest | Total |
|---|---|---|---|---|---|---|---|
| Class 1 (Sig. ↑ in A0) | 3072 (16) | 5888 (30) | 6528 (33) | 448 (2) | 3776 (19) | 0 (0) | 19712 (100) |
| Class 2 (Sig. ↑ in A0 & ↓ in P1 ) | 704 (4) | 3712 (20) | 10304 (56) | 256 (1) | 3584 (19) | 0 (0) | 18560 (100) |
| Class 3 (Sig. ↑ in A1) | 960 (14) | 704 (10) | 448 (7) | 64 (1) | 4672 (68) | 0 (0) | 6848 (100) |
| Class 4 (Sig. ↓ in A1) | 3520 (19) | 1792 (10) | 1024 (5) | 1216 (7) | 11008 (59) | 128 (1) | 18688 (100) |
| Class 5 (Sig. ↓ in P1) | 576 (4) | 2368 (16) | 7040 (48) | 128 (1) | 4352 (30) | 256 (2) | 14720 (100) |
| Not significant | 14144 (18) | 11328 (14) | 13568 (17) | 4160 (5) | 35008 (44) | 1344 (2) | 79552 (100) |
| Others (Small sig. changes) | 5376 (14) | 5504 (14) | 7872 (20) | 2112 (5) | 16576 (43) | 1024 (3) | 38464 (100) |

**Table 4.** The percentage of sub-basin's significant trend out of the total area of significant trend in the basin and the percentage of area significantly increasing or decreasing within sub-basins are shown. The locations of the sub-basins can be found in Fig. 8a.

| Sub-basins | % of total trend | | | % of sub-basin's area | | |
| --- | --- | --- | --- | --- | --- | --- |
| | Insignificant trend | Significantly greening | Significantly browning | Insignificant trend | Significantly greening | Significantly browning |
| Anger | 3.37 | 0.46 | 5.27 | 52.96 | 0.14 | 46.90 |
| Belles | 3.77 | 1.12 | 13.50 | 32.90 | 0.18 | 66.91 |
| Beshilo | 9.78 | 18.23 | 0.97 | 91.65 | 3.22 | 5.13 |
| Dabus | 8.76 | 5.07 | 14.27 | 51.68 | 0.56 | 47.76 |
| Didessa | 9.28 | 1.76 | 11.48 | 58.64 | 0.21 | 41.15 |
| Dinder | 6.78 | 0.18 | 9.19 | 56.54 | 0.03 | 43.43 |
| Finca | 2.66 | 2.96 | 0.96 | 81.62 | 1.71 | 16.67 |
| Guder | 4.85 | 7.61 | 1.15 | 85.87 | 2.54 | 11.59 |
| Jemma | 11.48 | 22.03 | 1.45 | 90.25 | 3.26 | 6.49 |
| Muger | 5.88 | 12.15 | 0.86 | 89.13 | 3.47 | 7.40 |
| North Gojam | 8.65 | 12.78 | 4.76 | 74.64 | 2.08 | 23.28 |
| Rahad | 2.64 | 0.01 | 7.10 | 39.59 | 0.00 | 60.41 |
| South Gojam | 8.43 | 3.88 | 8.84 | 62.37 | 0.54 | 37.09 |
| Tana | 5.11 | 1.89 | 8.11 | 52.45 | 0.37 | 47.18 |
| Welaka | 4.82 | 9.77 | 0.29 | 93.24 | 3.56 | 3.20 |
| Wonbera | 3.74 | 0.10 | 11.81 | 35.86 | 0.02 | 64.12 |
| Total | 100 | 100 | 100 | 63.05 | 1.19 | 35.76 |

**Table 5.** Summary statistics of Theil–Sen slope (median trend) for the significantly increasing (greening) and decreasing (browning) trends per sub-basins. Locations of the sub-basins can be found in Fig. 8a.

| Sub-basins | Significantly greening ($\Delta$ NDVI y$^{-1}$) | | | Significantly browning ($\Delta$ NDVI yr$^{-1}$) | | |
|---|---|---|---|---|---|---|
| | Minimum | Maximum | Mean | Minimum | Maximum | Mean |
| Anger | 0.0444 | 0.0984 | 0.0612 | 0.0336 | 0.1740 | 0.0768 |
| Belles | 0.0456 | 0.1524 | 0.0744 | 0.0348 | 0.1908 | 0.0816 |
| Beshilo | 0.0420 | 0.1596 | 0.0660 | 0.0384 | 0.1572 | 0.0660 |
| Dabus | 0.0432 | 0.1812 | 0.0768 | 0.0372 | 0.1764 | 0.0744 |
| Didessa | 0.0444 | 0.0984 | 0.0624 | 0.0312 | 0.2124 | 0.0792 |
| Dinder | 0.0372 | 0.0912 | 0.0552 | 0.0348 | 0.1692 | 0.0756 |
| Fincha | 0.0444 | 0.1524 | 0.0732 | 0.0372 | 0.1656 | 0.0708 |
| Guder | 0.0420 | 0.1176 | 0.0648 | 0.0360 | 0.1584 | 0.0684 |
| Jemma | 0.0408 | 0.1920 | 0.0660 | 0.0348 | 0.2016 | 0.0660 |
| Muger | 0.0432 | 0.1224 | 0.0648 | 0.0408 | 0.1464 | 0.0684 |
| North Gojam | 0.0372 | 0.1332 | 0.0660 | 0.0384 | 0.1704 | 0.0732 |
| Rahad | 0.0528 | 0.0660 | 0.0600 | 0.0384 | 0.1620 | 0.0756 |
| South Gojam | 0.0408 | 0.1308 | 0.0636 | 0.0356 | 0.1836 | 0.0768 |
| Tana | 0.0444 | 0.1476 | 0.0672 | 0.0372 | 0.2028 | 0.0792 |
| Welaka | 0.0348 | 0.1476 | 0.0660 | 0.0420 | 0.1488 | 0.0636 |
| Wonbera | 0.0504 | 0.1452 | 0.0696 | 0.0336 | 0.1884 | 0.0792 |
| Total | 0.0348 | 0.1920 | 0.0660 | 0.0312 | 0.2124 | 0.0768 |

**Table 6.** Change point analysis result using Pettitt's test.

| Variables | ROI#1 | ROI#2 | ROI#3 | ROI#4 | ROI#5 | ROI#6 | ROI#7 | ROI#8 |
|---|---|---|---|---|---|---|---|---|
| Annual mean NDVI (A0) | 2003 $(-)^{*}$ | 2004 $(-)^{***}$ | 2004 $(-)^{**}$ | 2007 $(+)^{**}$ | 2005 $(-)^{**}$ | 2003 $(-)$ | 2004 $(+)^{***}$ | 2005 $(-)^{***}$ |
| Annual amplitude (A1) | 2004 $(-)^{**}$ | 2006 $(-)^{***}$ | 2006 $(-)$ | 2007 $(+)^{*}$ | 2004 $(-)^{**}$ | 2006 $(-)^{*}$ | 2007 $(-)$ | 2005 $(-)^{***}$ |
| Semi-annual amplitude (A2) | 2004 $(-)$ | 2004 $(-)$ | 2006 $(-)$ | 2005 $(+)^{*}$ | 2004 $(-)$ | 2003 $(-)^{*}$ | 2007 $(-)^{**}$ | 2007 $(-)$ |

$^{*} = p < 0.1$
$^{**} = p < 0.05$
$^{***} = p < 0.001$
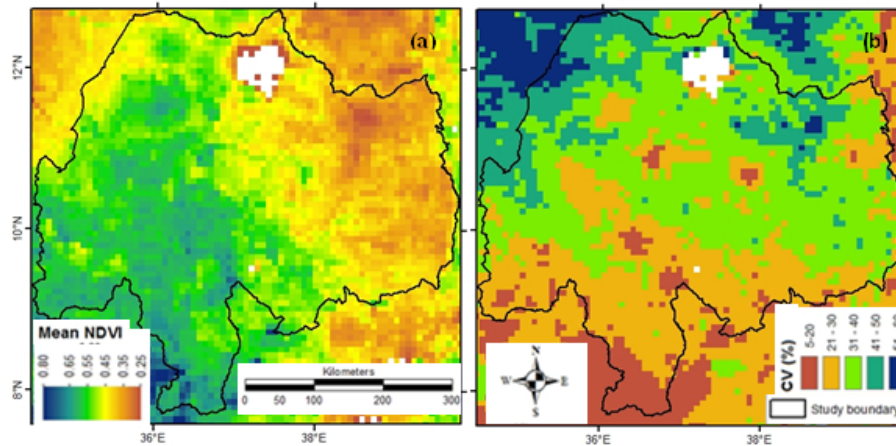
**Figure 1.** Spatial distribution of multi-year (1982–2006) mean monthly GIMMS NDVI **(a)** and coefficient of variation **(b)**.
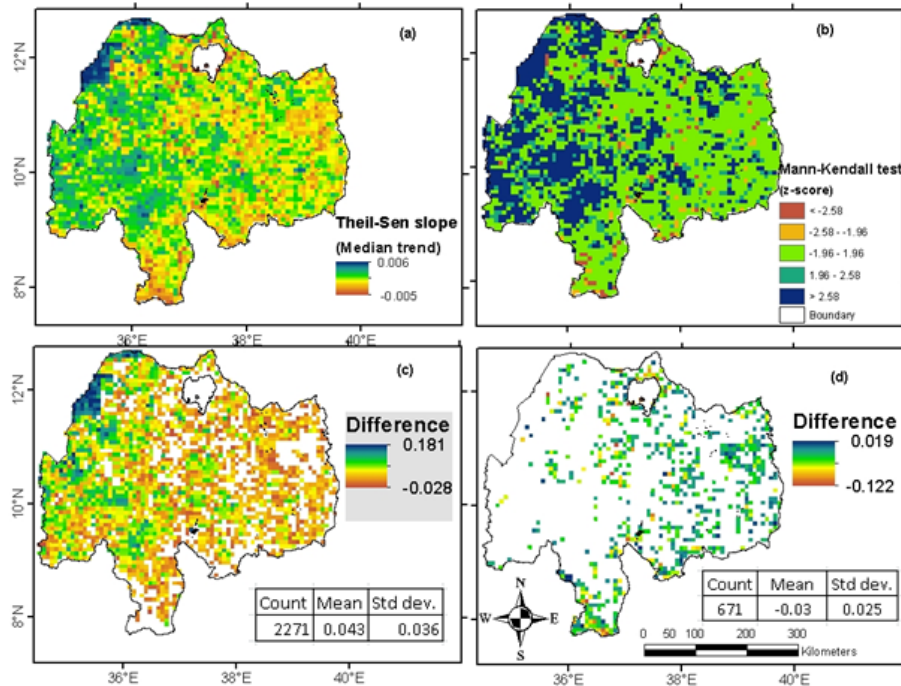
**Figure 2.** Per-pixel difference between linear trend test and non-linear monotonic (Mann–Kendall) trend test on NDVI in Abay (UBN) basin for the period 1982 to 2006): **(a)** median trend **(b)** Mann-Kendall significance test $Z$ score, **(c)** the spatial distribution map of per-pixel difference between linear trend test and non-linear monotonic (Mann–Kendall) trend test for areas of positive NDVI trends, and **(d)** the spatial distribution map of per-pixel difference between linear trend test and non-linear monotonic (Mann–Kendall (MK)) trend test for areas of negative NDVI trends. MK test values were subtracted from the linear test values.
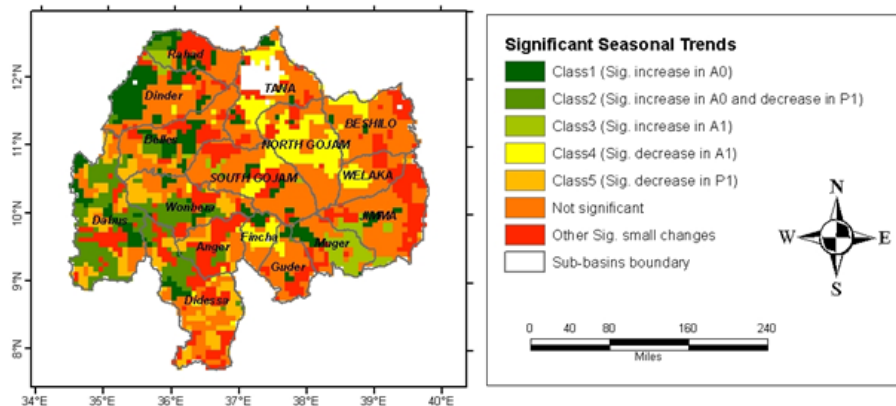
**Figure 3.** The five most prevalent classes of significant seasonal trends in GIMMS NDVI (1982–2006): Class 1 shows significant increases in Amplitude 0 (Mean NDVI); Class 2 shows significant increases in Amplitude 0 and decrease in Phase 1 together; Class 3 shows significant increases in Amplitude 1 (increase in the difference between minimum and maximum NDVI without affecting the mean); Class 4 shows significant decreases in Amplitude 1; and Class 5 shows significant decreases in Phase 1.

Title Page

Abstract | Introduction

Conclusions | References

Tables | Figures

Back | Close

Full Screen / Esc

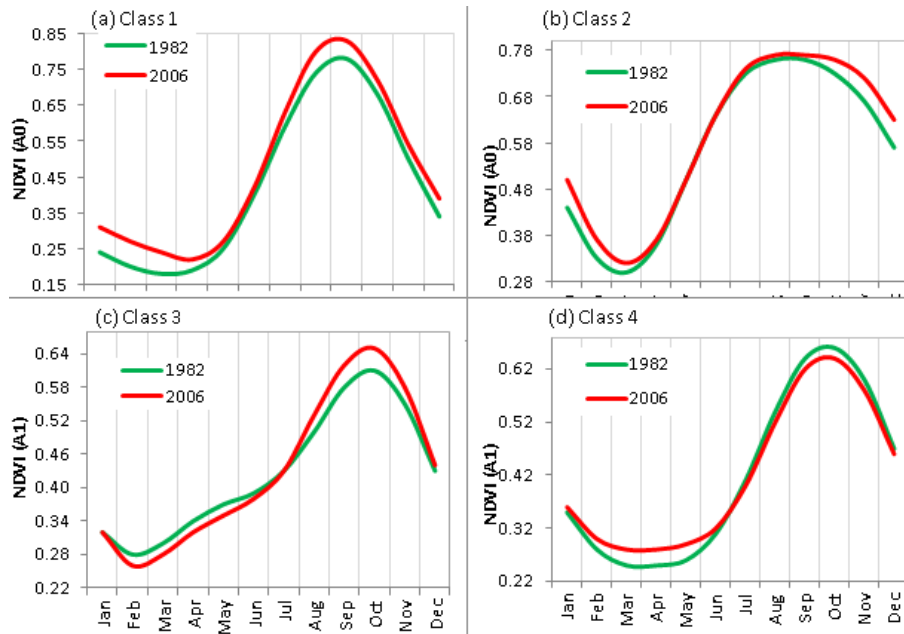Printer-friendly Version

Interactive Discussion

**Figure 4.** The seasonal trends representative of each of the major trend classes from the 1982–2006 series. The green curve represents the characteristic seasonal curve at the beginning of the series (1982) while the red curve represents the characteristic seasonal curve at the end of the series (2006). These are fitted curves, much like a regression trend line or a trend surface. They are not meant to provide a close fit to the actual curves for any specific year. Rather, their shape (and trend in shape) is derived from an analysis of the entire series – in this case 25 years. They are not intended as descriptions of 1982 and 2006 specifically, but rather (based on the full 25 years of data) the best fit modeled curves for 1982 and 2006, respectively.
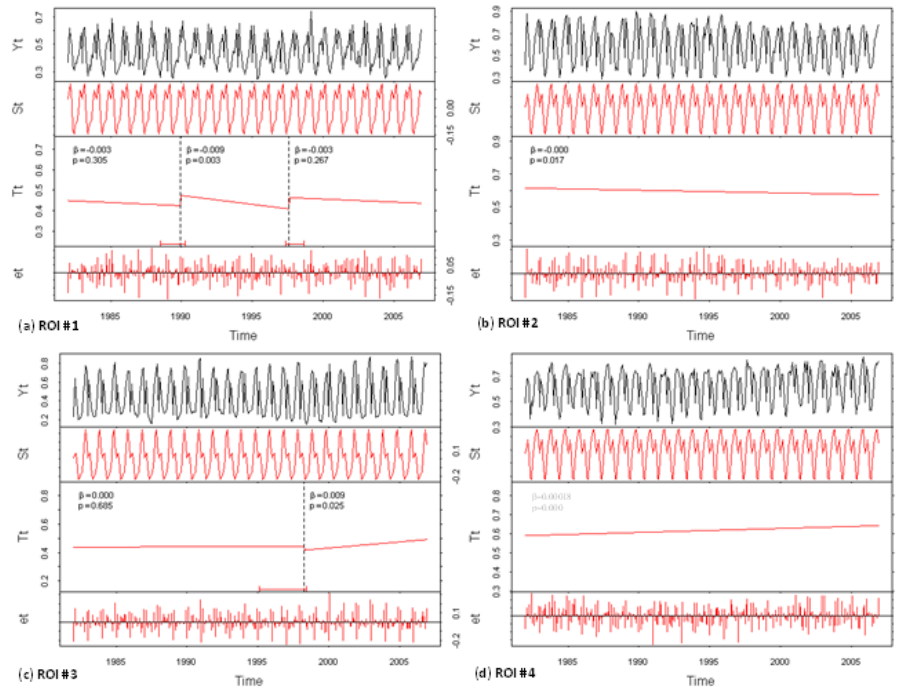
**Figure 5.** Examples of decomposition and trend break analysis of monthly GIMMS NDVI time series (1982–2006) for certain region of interests (ROIs) generated by BFAST approach **(a)** ROI #1 (37.8° E, 10.4° N), **(b)** ROI #2 (37.5° E, 9.8° N), **(c)** ROI #3 (37.6° E, 10.3° N), **(d)** ROI #4 (35.1° E, 9.3° N). The top panel in every plot shows the NDVI data ($Y_i$), whereas the other three panels depict the individual components after decomposition. The seasonal ($S_t$) and remainder ($e_t$) components have zero mean while the trend component ($T_t$) shows the trend in NDVI. The slope coefficients ($\beta$) and the significance levels ($P$) at $\alpha$ value of 0.05 for each segment are given.

**Figure 6.** Pettitt test's change point analysis of harmonic series shape parameters for: **(a)** Class 1 (significant increases in Amplitude 0 (Mean NDVI)); **(b)** Class 2 (significant increases in Amplitude 0 and decrease in Phase 1 together); **(c)** Class 3 (significant increases in Amplitude 1); and **(d)** Class 4 (significant decreases in Amplitude 1).

**Figure 7.** Vegetation cover variability and trends for the Upper Blue Nile (Abay) basin based on MODIS 250 mm NDVI (MOD13Q1) for the period (2001–2011): **(a)** multi-year mean monthly NDVI; **(b)** coefficient of variation of monthly NDVI; **(c)** Theil–Sen slope (Δ NDVI/month); and **(d)** Mann–Kendall (MK) significance test of the trend test.
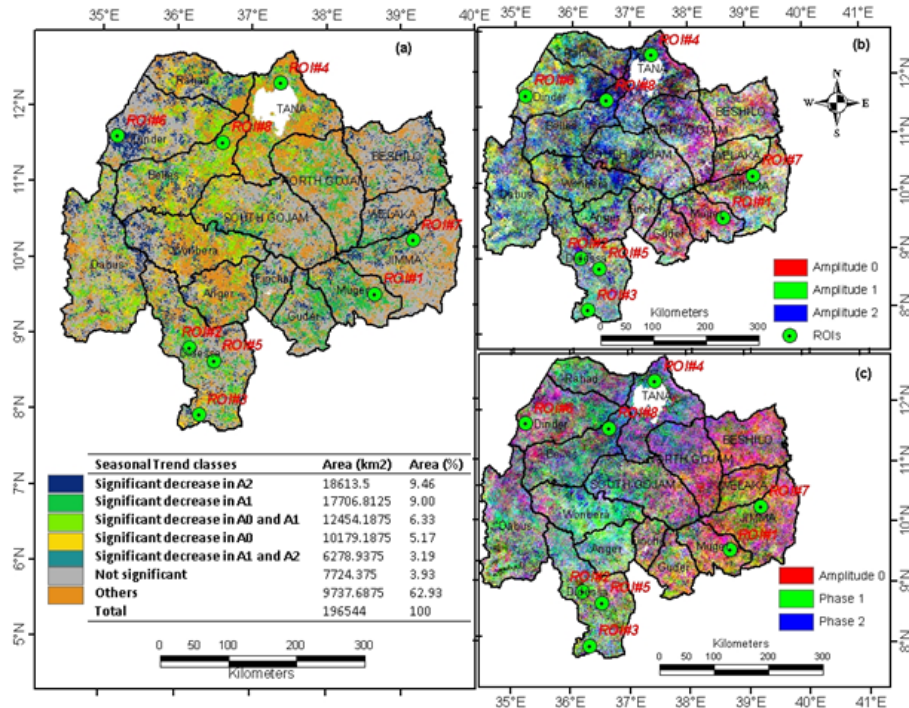
**Figure 8.** Results of the seasonal trends analysis of monthly 250 m MODIS NDVI (MOD13Q1) for the Upper Blue Nile/Abay basin from 2001 to 2011: **(a)** most prevalent classes of significant seasonal trends; **(b)** the amplitude trend composite, represents a color composite of the mean NDVI in red, the amplitude of 1 year in green and the amplitude of 6 months in blue; and **(c)** the phase trend composite. Areas that are going through similar trends in seasonality are shown by the colors.
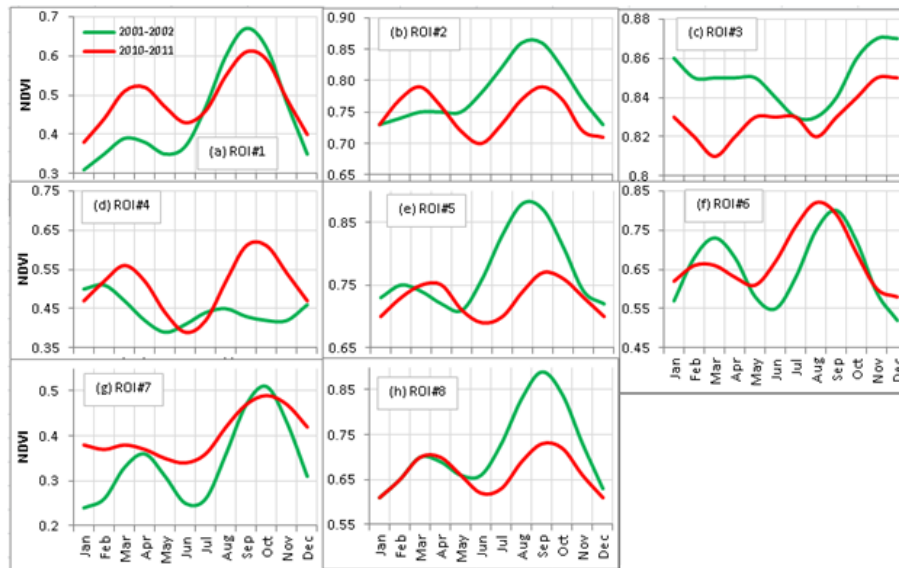
**Figure 9.** Fitted seasonal curves for 2001–2002 in green and 2010–2011 in red, derived from trends over the complete series. The intra-annual variations of generalized monthly NDVI over the first and last two-year periods of the time series (2001–2002 and 2010–2011) are shown for the 8 ROIs selected based on the amplitude composite images (Fig. 8b). The spatial patterns of the colors exhibit significant trends in one or more of the amplitude shape parameters (i.e. A0, A1 and A2) and depict different land use and climate conditions.

Full Screen / Esc

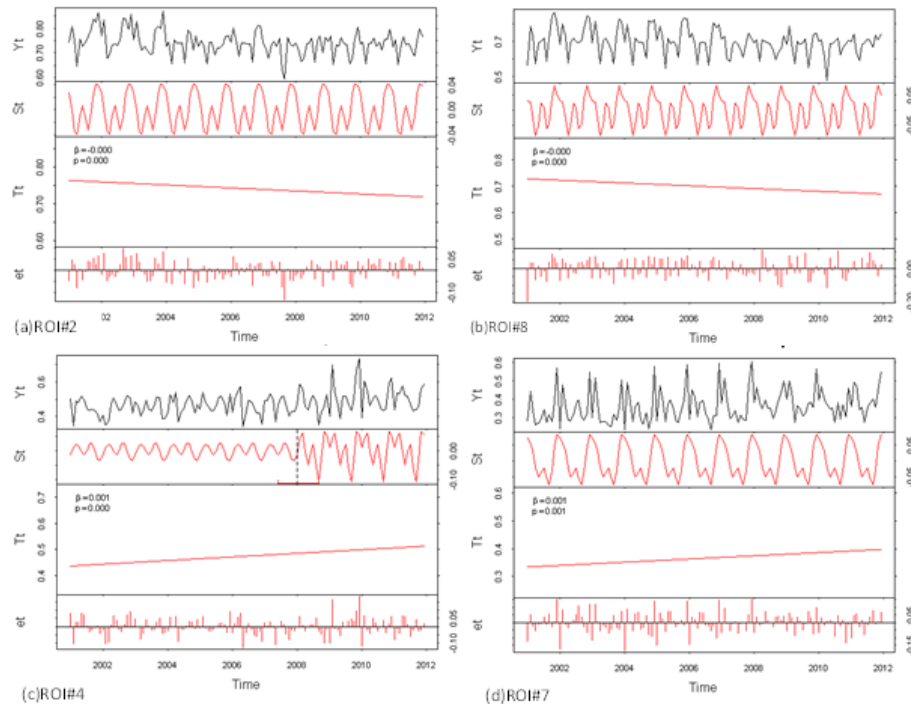Printer-friendly Version

Interactive Discussion



**Figure 10.** Examples of decomposition and trend break analysis of monthly MODIS NDVI time series (2001–2011) for certain region of interests (ROIs) for significant decreasing trends: **(a)** ROI #2 (37.8° E, 10.4° N) and **(b)** ROI #8 (37.5° E, 9.8° N) and for significant increasing trends: **(c)** ROI #4 (37.6° E, 10.3° N) and **(d)** ROI #7 (35.1° E, 9.3° N) generated by BFAST approach. The top panel in every plot shows the NDVI data ($Y_i$), whereas the other three panels depict the individual components after decomposition. The seasonal ($S_t$) and remainder ($e_t$) components have zero mean while the trend component ($T_t$) shows the trend in NDVI. The slope coefficients ($\beta$) and the significance levels ($P$) at $\alpha$ value of 0.05 for each segment are given.